Official journal of the CIOMP 2047-7538
www.nature.com/lsa

ARTICLE Open Access

High-performance terahertz modulators induced by substrate field in Te-based all-2D heterojunctions

Pujing Zhang[1], Qihang Liang[1], Qingli Zhou[1]✉, Jinyu Chen[1], Menglei Li[1], Yuwang Deng[1], Wanlin Liang[1], Liangliang Zhang[1], Qinghua Zhang[2], Lin Gu[3], Chen Ge[2]✉, Kui-juan Jin[2], Cunlin Zhang[1] and Guozhen Yang[2]

Abstract

High-performance active terahertz modulators as the indispensable core components are of great importance for the next generation communication technology. However, they currently suffer from the tradeoff between modulation depth and speed. Here, we introduce two-dimensional (2D) tellurium (Te) nanofilms with the unique structure as a new class of optically controlled terahertz modulators and demonstrate their integrated heterojunctions can successfully improve the device performances to the optimal and applicable levels among the existing all-2D broadband modulators. Further photoresponse measurements confirm the significant impact of the stacking order. We first clarify the direction of the substrate-induced electric field through first-principles calculations and uncover the unusual interaction mechanism in the photoexcited carrier dynamics associated with the charge transfer and interlayer exciton recombination. This advances the fundamental and applicative research of Te nanomaterials in high-performance terahertz optoelectronics.

Introduction

Terahertz (THz) technology has been considered as a potential candidate for the next generation communication system[1–3]. Wherein, high-performance modulator is one of the most significant components to load the information to the THz wave directly. However, the lack of suitable materials and effective active regulation has limited the development of this technology[4,5]. Two-dimensional (2D) materials with unique physical properties such as strong light-matter interactions, atomically thin profile, and fast carrier recombination, could offer an intriguing platform for investigating optoelectronic devices in fundamental physics[6–8]. Recently, the THz modulators based on 2D materials have attracted much attention with optical, magnetic, and electric control. Wherein, light field regulation provides higher degree of freedom and an easy access to tune the THz waves due to its rapid response and non-destructive contact[9–13]. At present, all-optically controlled THz modulator is faced with the tradeoff between modulation depth and speed, as well as the problem of insertion losses and bandwidth. Conventional semiconductor materials have high modulation depth but relatively slow modulation speed, which affects their development in ultrafast devices[14,15]. Although 2D materials have the transient response characteristics, the existing low modulation depth or the requirement of high pump fluence will hinder their practical applications[8,16,17]. Therefore, it is urgent to find out the favorable 2D materials to boost the device performances. The emerging mono-elemental 2D tellurium (Te) brings the dawn to this issue. This material with unique helical chain structure is of great superiorities, such as layer-dependent bandgap, extraordinarily high

Correspondence: Qingli Zhou (qlzhou@cnu.edu.cn) or
Chen Ge (gechen@iphy.ac.cn)
[1]Department of Physics, Key Laboratory of Terahertz Optoelectronics, Ministry of Education, and Beijing Advanced Innovation Center for Imaging Theory and Technology, Capital Normal University, Beijing 100048, China
[2]Beijing National Laboratory for Condensed Matter Physics, Institute of Physics, Chinese Academy of Sciences, Beijing 100190, China
Full list of author information is available at the end of the article

carrier mobility, strong optical response, and good air-stability[18–24].

In addition, the heterojunctions fabricated by easily stacking different 2D materials can break through the limitation of lattice matching, which is required in the bulk semiconductor heterojunctions[25–27]. In particular, the dangling-bond-free surfaces of 2D layered materials enable the formation of an atomically sharp interface with on-demand properties[28–30]. Furthermore, the typeII band alignment is conducive for the separation and transfer of the photocarriers[31,32]. This is crucial for the light-electric interconversion at the van der Waals (vdW) heterointerface in the optoelectronic applications. For example, the heterojunction of 2D Te and transition metal dichalcogenide can construct the highly-efficient solar cells[33]. Other infrared photodetectors using Te-based vdW heterojunctions achieved a high detectivity and fast response time[23,32]. However, few studies have been carried out on the high-performance THz modulators integrated with 2D Te heterojunctions. It is expected that such THz modulators can be regulated through heterojunction interface to provide an exploratory possibility for functional devices. Importantly, as a powerful technique to measure complex photoconductivity after optical excitation, THz wave can also probe the dynamics of free carriers or bounded excitons in a nondestructive way[9,34]. Our investigation of THz photodevices formed by all-2D Te-based heterojunctions could reveal the vdW interlayer coupling and the carrier dynamics. It is helpful to further understand the relationship between the heterointerface formation and substrate effect, facilitate the multi-parameter optimization of the modulation performance, and clarify the working principle of the novel THz devices.

Here, combined with substrate engineering, we have first proposed an efficient strategy to introduce Te-based nanofilms as a new class of optically controlled THz modulators. It is found that the low-loss and broadband Te nanofilms can achieve high modulation depth in a picosecond timescale and show an ultrasensitive response under low pump excitation. Further parameter optimization can be realized in their formed vdW heterojunctions. Especially, Ge/Te exhibits an enhanced modulation depth of 87.6% along with short-lived dynamics of less than 8 ps relaxation time that originates from the charge transfer and interlayer exciton recombination. Moreover, the measurements display the ohmic-like contact in Te/Ge but good rectifying behavior in Ge/Te, implying the stacking order can significantly modify the energy band structure induced by the substrate effect. By calculating the space distribution of the differential charge density with density functional theory (DFT), we first validate the existence of the substrate-induced electric field and clarify its influence on the charge transfer process of non-equilibrium state after photoexcitation. Our obtained results show the Te-based all-2D vdW heterojunctions with the substrate engineering can improve the device performances remarkably and open up a new idea for the design, optimization, and application of the optically controlled highly-efficient THz modulators.

Results

THz transient dynamic process of devices

High-quality and large-area Te nanofilms were deposited by the electron beam evaporation method on the fused silica substrates. The X-ray diffraction (XRD) pattern to examine the structure and crystalline nature is shown in Fig. 1a. Typical characteristic diffraction peaks of (101) and (110) for Te (PDF card no. 36-1452) can be detected. As presented in Fig. 1b, X-ray photoelectron spectroscopy (XPS) spectrum of Te nanofilm exhibits two obvious peaks with the binding energies of 573.2 and 583.9 eV, which are assigned to Te $3d_{5/2}$ and Te $3d_{3/2}$, respectively. The Raman spectrum is shown in Fig. 1c. The prominent peaks located at 94, 121, and 142 cm^{-1} can be attributed to the E_1, A_1, and E_2 vibration modes, which are caused by the asymmetric bond-stretching along *c*-axis and assigned to predominately bond-bending, chain expansion, and bond-stretching types, respectively[19–21,32]. To further confirm the crystal structure of different domains, high-resolution transmission electron microscopy was performed as displayed in Fig. 1d, which directly illustrates the crystalline state of Te layer and shows trigonal structure[20,22]. Other characterizations are presented in Fig. S1, showing the thickness is 100 nm with the optical bandgap of 0.37 ± 0.01 eV[35].

Our schematic experimental scheme is illustrated in Fig. 2a using optical pump-THz probe technology to investigate the active modulation response of Te-based THz devices[14]. The measured transient THz dynamics is demonstrated in Fig. 2b for Te (100 nm) with 800 nm pump excitation. The relative change is defined as $-\Delta T/T_0 = -(T - T_0)/T_0$, where T_0 and T are the THz peak values before and after the photoexcitation. It is found that $-\Delta T/T_0$ first shows a rapid positive change and reaches its maximum within several picoseconds after the photoexcitation owing to the generation of hot carriers[36,37]. The subsequent relaxation processes under different pump fluence are well fitted by the biexponential functions, and the extracted relaxation times τ_1 and τ_2 are displayed in Fig. 2c (see Table S1 for details). It is shown that the decay consists of two stages with distinct timescales. The fast recovery occurs within 2 ps, which represents the energy relaxation of the carriers. This pump-independent trend of τ_1 might originate from the electron-phonon scattering process[11]. Then a slow recovery lasts for about 8 ps to depict the carrier lifetime and its independence on pump fluence suggests that the

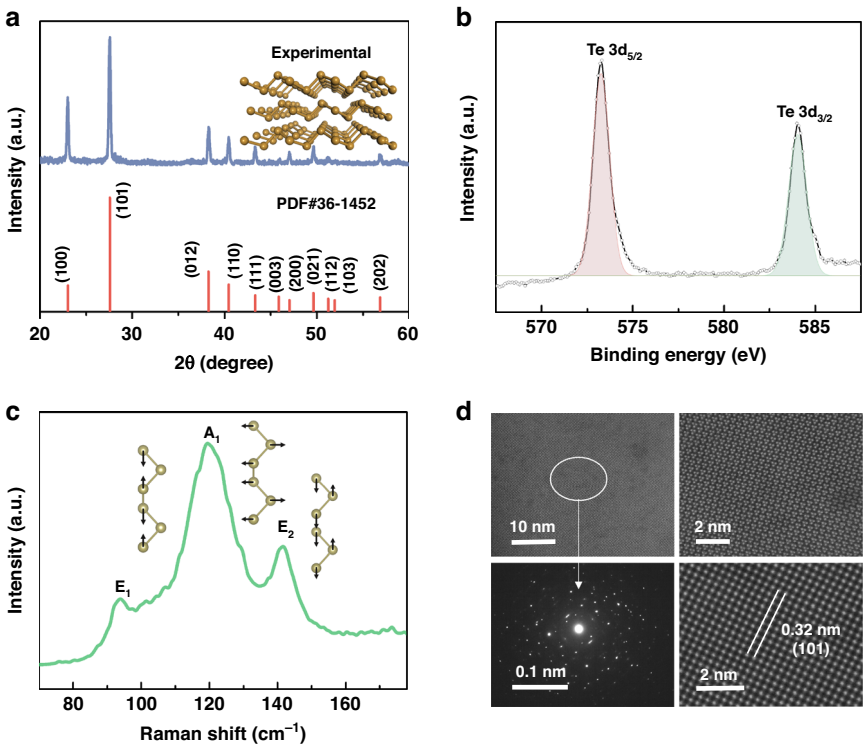

Fig. 1 Characterization of Te nanofilms. a XRD patterns. **b** XPS spectrum. **c** Raman spectrum. **d** HRTEM images. The measured lattice distance is 0.32 nm, corresponding to the (101) planes of Te crystal

synergistic interactions between Auger effect and defect trapping dominate the photocarrier dynamics of Te[38]. Therein, the recombination centers formed by impurities and defects promote recombination and shorten the carrier lifetime, while the formation of the trap center prolongs the lifetime. Under 400 nm pump excitation, the relaxation time constants remain unchanged (Supplementary Fig. S2). This feature is beneficial to accomplish the unperturbed modulation speed in the optical active devices since the carrier lifetime is usually deteriorated with the increased pump intensity. In addition, the transmitted THz wave can be significantly attenuated, which can be described by modulation depth of $MD = |-\Delta T/T_0|_{max}$. It can be seen that the MD of Te (100 nm) is 14.5% even at an extremely low fluence of 2.6 μJ cm^{-2} and can reach 65.3% at 260 μJ cm^{-2}. The corresponding transmission spectra at pump delay time of 0 ps exhibit the fluence-dependent but frequency-independent broadband features (Supplementary Fig. S3). It is worth noting that this material has a high transmission of 96.3% without pump, leading a very low insertion loss of −0.33 dB calculated by 20lg (E_{sam}/E_{sub}), where E_{sam} and E_{sub} are the THz amplitudes for sample and substrate, respectively. Different from the behaviors of Te (300 nm) with much longer carrier lifetime and Te (50 nm) with relatively low MD (Supplementary Fig. S4), Te (100 nm) is the optimal candidate to accomplish the excellent modulation characteristics. Furthermore, we calculate the skin depth of the pumped film at THz frequencies given in Fig. S4d, which confirms that the film can significantly suppress THz transmission. To better reveal the optical properties of Te (100 nm) in the THz region, we have calculated the complex photoconductivity with the real part σ_1 and imaginary part σ_2 displayed in Fig. 2d under different fluence at pump delay time of 0 ps. The modified Drude-Smith conductivity formula was derived with a more solid physical foundation and well-defined fit parameters[39]. This model, which is based on a diffusive restoring current to provide a direct connection between THz conductivity and microscopic particle motion, can be expressed by $\tilde{\sigma}(\omega) = \frac{Ne^2\tau'}{m(1-i\omega\tau')}\left[1 - \frac{1}{1-i\omega t_d}\right]$, where N, e, m, ω, τ', and t_d are charge carrier density, elementary charge, effective mass, plasma frequency, total scattering time, and diffusion time, respectively[39–41]. The fitted curves in Fig. 2d exhibit a good agreement with experimental data. The fitting parameters are given in Table S2. It is found that the carrier total scattering time (τ') reduces from 750 to 375 fs and diffusion time (t_d) rises from 21 to 53 fs due to the enhancement of carrier concentration with the increased pump fluence[35,42,43].

Since the heterointerface could enhance the photoelectric conversion efficiency, the Te-based heterojunctions

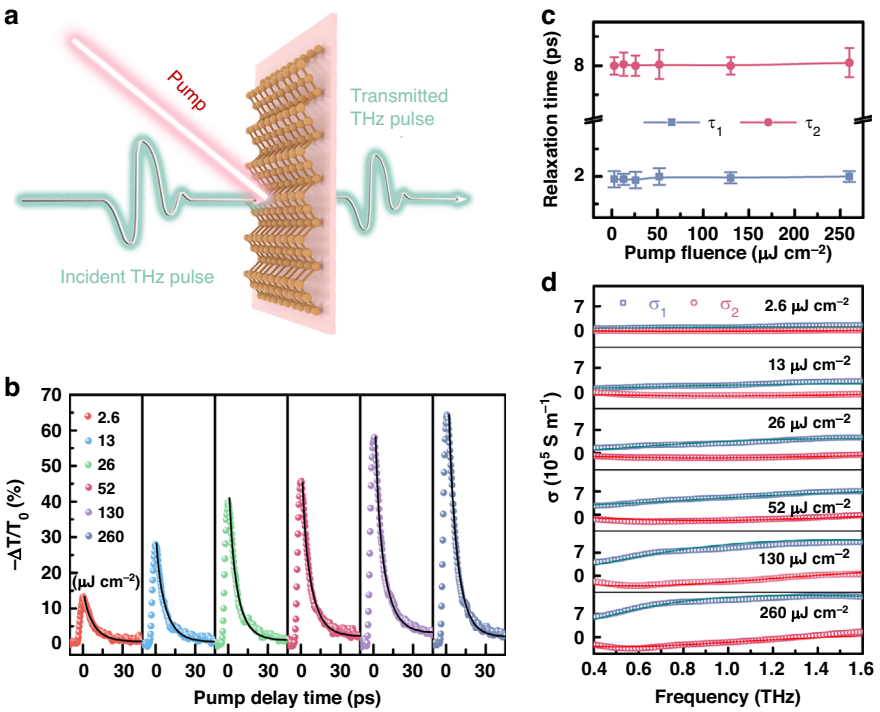

Fig. 2 Transient dynamics properties of Te. a Schematic illustration of THz measurement scheme. **b** Transient THz dynamics of Te (100 nm) under different pump fluence with 800 nm excitation wavelength. Black solid lines represent the biexponential fitting curves. **c** Pump fluence dependence of the fitted relaxation times. **d** Measured complex photoconductivity spectra. Solid lines represent the Drude-Smith fitting curves

are expected to further improve the performance of devices. Firstly, we have studied the THz responses of heterojunctions formed by Te (100 nm) and monolayer graphene (Gr) in different stacking orders. Figure 3a demonstrates $-\Delta T/T_0$ at the peak of THz amplitude for Gr and Te, Te/Gr and Gr/Te heterojunctions under 800 nm pump with the fixed fluence of 26 μJ cm^{-2}. It is known that Gr exhibits negative THz photoconductivity, which is ascribed to the enhancement of carrier scattering rate overtaking the increase in Drude weight[6]. The obtained positive THz photoconductivities of Te, Te/Gr, and Gr/Te indicate the main contribution from the free carriers. Moreover, relaxation processes still have two distinct decay components. It is obvious that when Gr and Te are combined into the heterojunction, the transient response does not decrease but slightly increases, showing that the heterointerface plays an important role in the carrier dynamics. Here, the photon excitation creates free carriers, and these charged carriers will rapidly transfer between the two layers. The black solid lines are the biexponential fitting of $-\Delta T/T_0$ at the peak of THz amplitude. The extracted time constants are $\tau_1 = 1.95 \pm 0.12$ ps and $\tau_2 = 8.00 \pm 0.25$ ps in Te, $\tau_1 = 1.85 \pm 0.15$ ps and $\tau_2 = 7.80 \pm 0.20$ ps in Te/Gr, $\tau_1 = 1.80 \pm 0.15$ ps and $\tau_2 = 7.90 \pm 0.25$ ps in Gr/Te, respectively. The slight decrease of in relaxation times in two heterojunctions suggests the possibility of exciton existence[16,26,30].

To further clarify the charge species and the transfer in the heterojunction, we can monitor the photoinduced dynamics of excitons since the THz photon allows it to couple with the intraexcitonic transition of bounded charge. In experiments, this can be quantified by scanning the change of the THz amplitude at a zero-crossing point (Supplementary Fig. S5), through which one is able to exclude the contribution of the photoinduced amplitude change[9,11,12,26]. The obtained transient curves presented in Fig. 3a depict the exciton dynamics fitted with red solid lines, displaying the exciton formation and annihilation via recombination to finally determine an exciton lifetime. We have found that the exciton lifetimes of Te, Te/Gr, and Gr/Te are significantly shorter than those of free carriers (Supplementary Table S3) due to the contribution from weak excitons. Especially, the lifetimes of both free carriers and excitons in the heterojunctions are further slightly reduced accompanied with the emergence of increased exciton component, indicating that electron-hole pairs are not only in the individual layers but also across the interface as the interlayer excitons. Thus, the picosecond carrier lifetimes are assigned to the charge transfer through the interface and subsequent interlayer exciton decay. The extracted *MD* under various fluence is

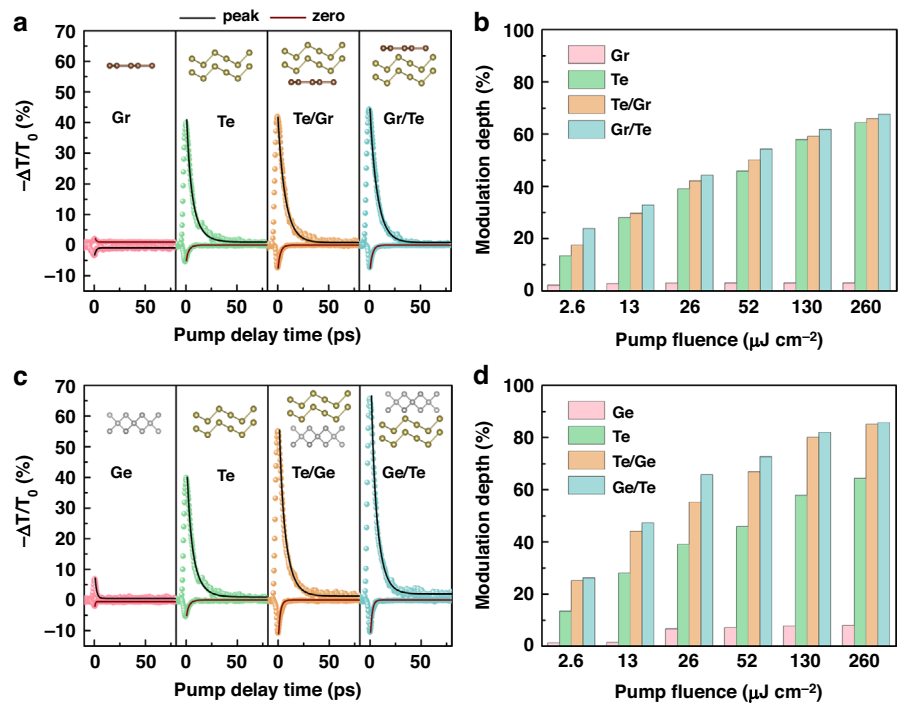

Fig. 3 Transient dynamics properties of Te-based heterojunctions. a $-\Delta T/T_0$ at the peak and zero crossing of THz amplitude under 800 nm pump with fluence of 26 μJ cm^{-2} and (**b**) fluence-dependent modulation depths for Gr and Te, Te/Gr and Gr/Te heterojunctions, as well as (**c**, **d**) for Ge and Te, Te/Ge and Ge/Te heterojunctions, respectively

presented in Fig. 3b. It can be seen with the increased pump fluence, the *MD* of Gr quickly reaches saturation with relatively low value of 2.8%. Compared with that of Te, the *MD*s of two heterojunctions are higher and exhibit larger difference at low fluence. Furthermore, the stacking order of Gr and Te has the obvious influence on the modulation property. It has been mentioned above that the *MD* of Te is 14.5% at pump fluence of 2.6 μJ cm^{-2} but Gr/Te can reach 23.5%, verifying the great potential of all-2D heterojunction to realize the modulation enhancement. At pump fluence of 260 μJ cm^{-2}, the value of Gr/Te is 69.0% with little difference from that of Te, suggesting the limited enhancement with the use of Gr and Te at high fluence.

It is known that the optical properties of the heterojunction are closely related to the material component and its interface. As an indirect band gap semiconductor, Ge has considerable potentials and can form the heterostructure with Te to improve device performance. Hence, we have further studied the THz transient responses of all-2D vdW heterojunctions formed by Te (100 nm) and Ge (100 nm). Figure 3c shows $-\Delta T/T_0$ at the peak and zero crossing of THz amplitude for Ge, Te, Te/Ge, and Ge/Te at 800 nm with pump fluence of 26 μJ cm^{-2}. The transient behavior of Ge/Gr and Gr/Ge is given in Fig. S6 for comparison. We can find that the optical excitation behavior is not significant in Ge with the negligible proportion of excitons. However, the photoexcited phenomena of Te/Ge and Ge/Te heterojunctions are more remarkable than those of not only individual component material but also the above Te/Gr and Gr/Te heterojunctions. The extracted time constants are $\tau_1 = 1.60 \pm 0.10$ ps and $\tau_2 = 7.70 \pm 0.20$ ps in Te/Ge, $\tau_1 = 1.50 \pm 0.10$ ps and $\tau_2 = 7.75 \pm 0.25$ ps in Ge/Te, respectively. Compared with the heterojunctions formed with Gr, those shorter relaxation times of free carriers and excitons (Supplementary Table S3) are the evidence of ultrafast and highly efficient charge transfer across the interface and the subsequent interlayer exciton decay. Moreover, the *MD* at 26 μJ cm^{-2} is significantly enhanced with the value of 55.4% for Te/Ge and 69.5% for Ge/Te, respectively. Figure 2d presents their *MD*s under different fluence. Wherein, the *MD* of Ge is also very small and insignificant because it only reaches 8.3% at high pump fluence. When Ge and Te are combined to form heterojunction, the *MD* increases considerably. Especially, the *MD* of our all-2D Ge/Te heterojunction can achieve 27.8% under the extremely low pump fluence of 2.6 μJ cm^{-2} and further accomplish an ultrahigh value of 87.6% at 260 μJ cm^{-2}, which is one of the key results of this work compared with other reported 2D modulators, as shown in Table 1[13,26,27,36,38,44]. This implies that Ge/Te

Table 1 Comparison between our work and other 2D THz modulators

2D material	Tuning methods	Pump wavelength	Modulation speed	*MD* @ low fluence	*MD* @ high fluence
CdTe[13]	Optical	400 nm (3.1 eV)	ps	2.3% (29 μJ cm^{-2})	9.5% (174 μJ cm^{-2})
$PtTe_2$[44]	Optical/Thermal	780 nm (1.59 eV)	ps	12% (60 μJ cm^{-2}@5 K)	27% (362 μJ cm^{-2}@5 K)
$PdSe_2$[38]	Optical/Thermal	780 nm (1.59 eV)	ps	1.1% (72 μJ cm^{-2})	2.4% (192 μJ cm^{-2}@100 K)
Cd_3As_2/CdTe[36]	Optical	800 nm (1.55 eV)	ps	12.3% (6.35 μJ cm^{-2})	80% (2500 μJ cm^{-2})
$MoTe_2$/WTe_2[26]	Optical	1550 nm (0.8 eV)	sub-ps	7.5% (10 μJ cm^{-2})	——
Graphene/$PtSe_2$[27]	Optical	1300 nm (0.95 eV)	ps	0.5% (9 μJ cm^{-2})	2.2% (362 μJ cm^{-2})
Te (this work)	Optical	800 nm (1.55 eV)	ps	14.5% (2.6 μJ cm^{-2})	65.3% (260 μJ cm^{-2})
Ge/Te (this work)	Optical	800 nm (1.55 eV)	ps	27.8% (2.6 μJ cm^{-2})	87.6% (260 μJ cm^{-2})

vdW heterojunction can effectively enhance the modulation depth while maintaining the fast speed, which may be due to the effect of stacking order on charge transfer and interlayer coupling.

Photoresponse properties of devices

To explore the physical mechanism of the stacking effect on the device performances, we measured the photoelectric responses to provide the interface information related with ultrafast behavior and modulation capability. The I–V curves of Te, Te/Ge and Ge/Te heterojunctions are presented in Fig. 4a under dark and light conditions. The linear relationship indicates the ohmic contact formed at their interface between Te nanofilm and Ag electrodes, as well as Ge and its electrodes (not shown). Notably, for the Te/Ge heterojunction, we also find the linear characteristic like ohmic contact, suggesting there is no obvious potential barrier at the formed Te/Ge heterointerface. However, I–V curve of Ge/Te is nonlinear with rectifying behavior, showing the emergence of barrier at their interface[19,32]. Figure 4b depicts their transient current response under 375 nm light irradiation. When the illumination is repeatedly turned on and off with on/off = 10/10 s, the presented eight cycles of 'on-off' state switching retain similar photocurrent, suggesting high stability and repeatability of device[24,32]. It can be found the photocurrent recoveries in two heterojunctions are more rapid, especially for Ge/Te. We further prolong the on/off time to 60/60 s to measure the photoresponse under the irradiation of 375 and 650 nm laser with different powers, as shown in Figs. 4c, d, respectively. It is also revealed that only the Ge/Te heterojunction can switch quickly between low and high current states with steep rise and fall edges, indicating that electron-hole pairs could be effectively transferred and recombined. This coincides with the efficient charge transfer and strong coupling between Ge and Te through the interface. Such dynamical response difference is of great importance for the design and fabrication of vdW heterostructures.

Theoretical analysis of substrate-induced carrier dynamics

Here, we assume that the effective field of the substrate engineers the band structure of the heterogeneous interface through the stacking order, and thus the optical transient behaviors can be regulated. According to the calculated electronic band structures of Ge and Te in Fig. 5a, we illustrate energy band diagrams of heterojunction in Fig. 5b (see calculation details in Supplementary Information). The electron affinity and bandgap are about 4.13 eV and 0.66 eV for Ge, and 4.02 eV and 0.37 eV for Te[19–21,45,46]. Due to the natural defects formed in the growth process, Te and Ge are usually weak *p*- and *n*-type semiconductors, respectively, with the Fermi levels near their individual intrinsic Fermi levels[19,21,46]. It can be seen that both the conduction band minimum (E_c) and the valence band maximum (E_v) of Te are higher than those of Ge with the type-II heterostructure. The photogenerated electrons in Te can be transferred to Ge layer through thermionic emission across the barrier. Meanwhile, the holes in Ge will move to Te. Hence, the interlayer exciton can be formed at the interface layer. When considering the effective electric field introduced by the substrate, the stacking order will cause the Fermi level shifting in Ge or Te layer. We have calculated the space distribution of the differential charge density between our used 2D materials and the fused silica substrate using DFT, as displayed in the left of Fig. 5c. The calculation results indicate that the direction of the effective electric field points to the substrate, leading to an electron accumulation layer at the side of the 2D material[47,48]. For Te/Ge, the substrate effect could shift the Fermi level of Ge upward to be close to that of Te. This will induce the reduction of the interface barrier to form the ohmic-like contact, which is consistent with the measured linear current in Fig. 4a. On the other hand, the substrate-induced effect can raise the Fermi level of Te, leading to the increased barrier at the interface of the Ge/Te heterojunction with prominent rectification characteristics. This can be also proved

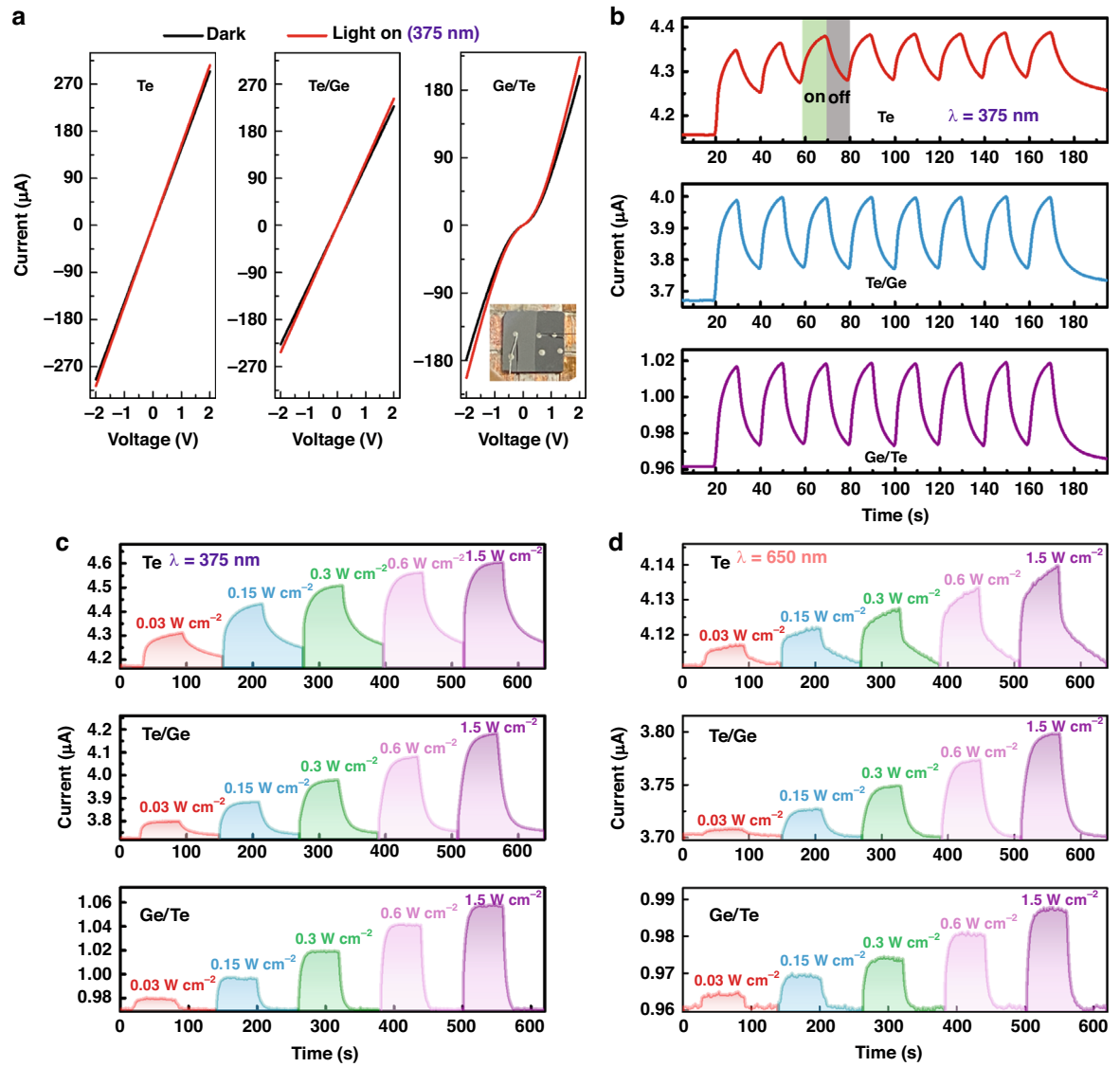

Fig. 4 Photoresponse measurements of Te, Te/Ge and Ge/Te heterojunctions. a I–V curves of Te, Te/Ge and Ge/Te heterojunctions in dark and light conditions (375 nm 0.3 W cm^{-2}), respectively. The inset shows the optical photo of Ge/Te heterostructure. **b** Time-resolved photoresponses of the samples under 375 nm with 0.3 W cm^{-2} (on/off = 10/10 s) at V_{bias} of 0.1 V. **c** Photo-switching characteristics measured at V_{bias} of 0.1 V under 375 nm and (**d**) 650 nm with different light powers (on/off = 60/60 s), respectively

by the surface potential difference between Te and Ge measured by AFM (Supplementary Fig. S7)[32].

Furthermore, the different optical modulation performances of those two heterostructures can be also described by the substrate field effect across the interfaces, as illustrated in the right of Fig. 5c. Here, we consider that the photogenerated carriers in Te play a dominant role after light excitation. For Te/Ge, the photoexcited holes can be transferred from the top Te to the bottom Ge under the effective electric field of the substrate. However, this process is extremely limited due to the large barrier in the valence band. For Ge/Te, the substrate induced electric field can significantly promote the transfer of photoexcited electrons from bottom Te to top Ge since their barrier in conduction band is relatively small with the permission of thermionic emission, thus increasing the THz photoconductivity. Simultaneously, the formation of interlayer excitons is promoted to shorten the carrier lifetime. It is noticed that this substrate-induced effect has a great impact on the charge transfer process under low pump photoexcitation[27]. Under high pump fluence, the excess photocarriers could partially screen the electric field, leading to the less influence of stacking order on modulation depth. Our obtained results indicate

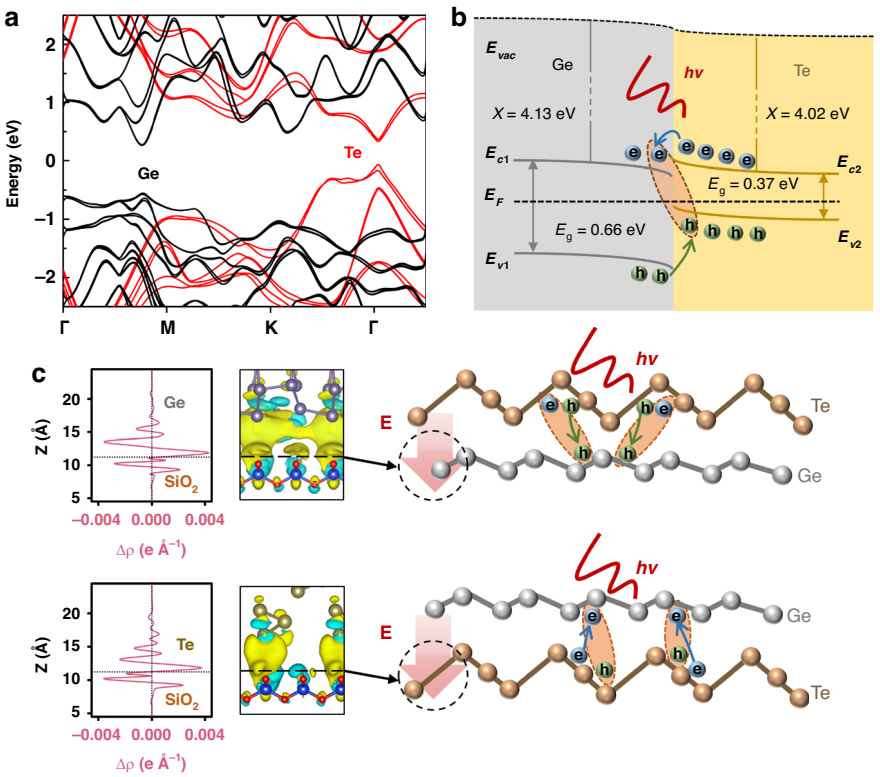

Fig. 5 Substrate-induced carrier dynamics in Te/Ge and Ge/Te heterojunctions. a Calculated band structures and (**b**) Energy band diagram of Ge and Te. **c** Left: Calculated space distribution of the differential charge density for different materials on substrate. The color blue (yellow) denotes electron depletion (accumulation). Right: Schematic substrate-induced electric fields and charge transfer in heterojunctions of Te/Ge (upper) and Ge/Te (lower), respectively

the substrate engineering can effectively improve the device performances in all-2D THz modulators.

Discussion

In summary, in view of the tradeoff between optical modulation depth and speed in the THz modulators, we have first proposed an approach to use the novel Te nanofilms combined with the heterostructure to promote device performances. The pure film modulator with low insertion loss and broadband width can achieve high modulation at the picosecond timescale and exhibit the ultrasensitive optical response at low excitation fluence. It is found that the highly efficient charge transfer and the formation of interlayer weak excitons at the heterointerface can enhance the modulation with the maintained ultrafast behavior. In particular, the Ge/Te vdW heterojunction achieves an ultrahigh *MD* of 87.6% with the shortened relaxation time of less than 8 ps and suggests the great influence of stacking order. Further photoresponse experiments exhibit the obvious rectification effect in Ge/Te due to the interface barrier. The subsequent DFT calculation and analysis first clarify the substrate-induced field could engineer the band structure to support the thermionic emission and the formation of interlayer excitons, thereby improving the ultrafast modulation properties. Our obtained results could provide a more comprehensive understanding on the internal mechanism of ultrafast charge transfer and exciton dynamics in all-2D heterostructures, guide the design of vdW interfaces, and envision a new class of power-efficient, high speed, low insertion loss, and broadband tunable THz photonic devices.

Materials and methods

Sample preparation

Te nanofilms were grown on the fused silica substrates in an electron-beam evaporator (VZS 600 Pro) with an in situ thickness meter. Before the deposition, fused silica substrates were cleaned by ultrasonication in acetone for 10 min and rinsed with isopropyl alcohol and deionized water. The deposition of Te was initiated from a 99.999% pure Te source in a boron nitride crucible at a rate of 0.1 nm s^{-1} under 10^{-4} Pa pressure. Annealing was performed in a tube furnace at 373 K under a 100 sccm Ar atmosphere for 0.5 h. Monolayer Gr and Ge nanofilms from SixCarbon Technology (Shenzhen, China) were transferred onto the prepared samples.

Material characterization

XRD patterns was performed using a Rigaku SmartLab instrument with a 2θ range from 20 to 80° in step of 0.05°. XPS measurements were performed on ThermoFisher Scientific ESCALAB 250X under monochromatic Al Kα radiation with an energy of 1486.6 eV. Raman spectrum was analyzed using the alpha300 R microscope under 532 nm laser excitation. The surface morphology of 2D Te was measured using Dimension ICON atomic force microscope and FEI Sirion scanning electron microscope. Absorption spectrum was performed using the Cary7000 UV-VIS-NIR Spectrophotometer.

Devices of photoresponse studies

Photoresponse were measured in a Lakeshore probe station with a Keithley 4200 semiconductor parameter analyzer in air at room temperature. The laser with a wavelength of 375 nm and 650 nm were used for the optical switching in the experiment.

Acknowledgements

This work was supported by the National Natural Science Foundation of China (Nos. 62075142, 12074271, 12074416, and 12222414) and the Youth Innovation Promotion Association of CAS (No. Y2022003). We would like to thank Prof. Xi-Cheng Zhang for discussion and comment.

Author details

[1]Department of Physics, Key Laboratory of Terahertz Optoelectronics, Ministry of Education, and Beijing Advanced Innovation Center for Imaging Theory and Technology, Capital Normal University, Beijing 100048, China. [2]Beijing National Laboratory for Condensed Matter Physics, Institute of Physics, Chinese Academy of Sciences, Beijing 100190, China. [3]Department of Materials Science and Engineering, Beijing National Center for Electron Microscopy and Laboratory of Advanced Materials, Tsinghua University, Beijing 100084, China

Author contributions

Q.Z. initiated the research. Q.Z. and C.G. supervised the project. The sample preparation, the device fabrication, and the device measurement were done by P.Z. with support from J.C. and C.G. First-principles calculations were performed by Q.L. and M.L. Q.Z. and P.Z. wrote the manuscript. C.G., Y.D., L.Z., Z.Z., L.G., K.J., C.Z. and G.Y. participated in the discussion and comment on the manuscript.

Data availability

All relevant data are available within the Article and Supplementary Information, or available from the corresponding authors upon reasonable request.

Competing interests

The authors declare no competing interests.

Supplementary information The online version contains supplementary material available at https://doi.org/10.1038/s41377-024-01393-6.

Received: 3 August 2023 Revised: 17 January 2024 Accepted: 21 January 2024
Published online: 05 March 2024

References

1. Ferguson, B. & Zhang, X. C. Materials for terahertz science and technology. *Nat. Mater.* **1**, 26–33 (2002).
2. Degl'Innocenti, R., Lin, H. & Navarro-Cía, M. Recent progress in terahertz metamaterial modulators. *Nanophotonics* **11**, 1485–1514 (2022).
3. Harter, T. et al. Generalized Kramers–Kronig receiver for coherent terahertz communications. *Nat. Photonics* **14**, 601–606 (2020).
4. Petrov, N. V. et al. Design of broadband terahertz vector and vortex beams: I. Review of materials and components. *Light. Adv. Manuf.* **3**, 54 (2022).
5. Petrov, N. V. et al. Design of broadband terahertz vector and vortex beams: II. Holographic assessment. *Light. Adv. Manuf.* **3**, 44 (2022).
6. Jnawali, G. et al. Observation of a transient decrease in terahertz conductivity of single-layer graphene induced by ultrafast optical excitation. *Nano Lett.* **13**, 524–530 (2013).
7. Sensale-Rodriguez, B. et al. Broadband graphene terahertz modulators enabled by intraband transitions. *Nat. Commun.* **3**, 780 (2012).
8. Sun, Z. P., Martinez, A. & Wang, F. Optical modulators with 2D layered materials. *Nat. Photonics* **10**, 227–238 (2016).
9. He, C. et al. Competition between free carriers and excitons mediated by defects observed in layered WSe_2 crystal with time-resolved terahertz spectroscopy. *Adv. Opt. Mater.* **6**, 1800290 (2018).
10. Motti, S. G. et al. Phase segregation in mixed-halide perovskites affects charge-carrier dynamics while preserving mobility. *Nat. Commun.* **12**, 6955 (2021).
11. Xing, X. et al. Role of photoinduced exciton in the transient terahertz conductivity of few-layer WS_2 laminate. *J. Phys. Chem. C.* **121**, 20451–20457 (2017).
12. Wang, F. et al. Exciton polarizability in semiconductor nanocrystals. *Nat. Mater.* **5**, 861–864 (2006).
13. Zhang, W. J. et al. Optically controlled ultrafast terahertz switching in a CdTe nanostructure thin film. *Appl. Opt.* **58**, 8200–8206 (2019).
14. Zhang, P. J. et al. Ultrahigh modulation enhancement in all-optical Si-Based THz modulators integrated with gold nanobipyramids. *Nano Lett.* **22**, 1541–1548 (2022).
15. Beard, M. C., Turner, G. M. & Schmuttenmaer, C. A. Transient photoconductivity in GaAs as measured by time-resolved terahertz spectroscopy. *Phys. Rev. B* **62**, 15764–15777 (2000).
16. Yu, Y. et al. Ultrafast formation and dynamics of interlayer exciton in a large-area CVD-grown WS_2/WSe_2 heterostructure. *J. Phys. Condens. Matter* **30**, 495701 (2018).
17. Gopalan, P. & Sensale-Rodriguez, B. 2D materials for terahertz modulation. *Adv. Opt. Mater.* **8**, 1900550 (2020).
18. Zhou, D. C. et al. Epitaxial growth of main group monoelemental 2D materials. *Adv. Funct. Mater.* **31**, 2006997 (2021).
19. Zheng, B. N. et al. Large-area tellurium/germanium heterojunction grown by molecular beam epitaxy for high-performance self-powered photodetector. *Adv. Opt. Mater.* **9**, 2101052 (2021).
20. Zhao, C. S. et al. Evaporated tellurium thin films for p-type field-effect transistors and circuits. *Nat. Nanotechnol.* **15**, 53–58 (2020).
21. Shi, Z. et al. Two-dimensional tellurium: progress, challenges, and prospects. *Nano-Micro Lett.* **12**, 99 (2020).
22. Shen, J. B. et al. Elemental electrical switch enabling phase segregation–free operation. *Science* **374**, 1390–1394 (2021).
23. Chitara, B. et al. Probing charge transfer in 2D MoS_2/tellurene type-II p–n heterojunctions. *MRS Commun.* **11**, 868–872 (2021).
24. Zhu, Z. L. et al. Multivalency-driven formation of Te-based monolayer materials: a combined first-principles and experimental study. *Phys. Rev. Lett.* **119**, 106101 (2017).
25. Liu, Y. et al. Van der Waals heterostructures and devices. *Nat. Rev. Mater.* **1**, 16042 (2016).
26. Lee, K. et al. Sub-picosecond carrier dynamics induced by efficient charge transfer in $MoTe_2$ /WTe_2 van der Waals Heterostructures. *ACS Nano* **13**, 9587–9594 (2019).
27. Ma, Q. S. et al. Hot carrier transfer in a Graphene/$PtSe_2$ heterostructure tuned by a substrate-introduced effective electric field. *J. Phys. Chem. C.* **125**, 9296–9302 (2021).
28. Choi, W. et al. Optoelectronics of multijunction heterostructures of transition metal dichalcogenides. *Nano Lett.* **20**, 1934–1943 (2020).
29. Liu, Y., Huang, Y. & Duan, X. F. Van der Waals integration before and beyond two-dimensional materials. *Nature* **567**, 323–333 (2019).
30. Yang, J. et al. Identifying the intermediate free-carrier dynamics across the charge separation in monolayer $MoS_2/ReSe_2$ heterostructures. *ACS Nano* **15**, 16760–16768 (2021).
31. Zhang, K. N. et al. Interlayer transition and infrared photodetection in atomically thin type-II $MoTe_2/MoS_2$ van der Waals Heterostructures. *ACS Nano* **10**, 3852–3858 (2016).

32. Cao, X. H. et al. Non-Layered Te/In_2S_3 tunneling heterojunctions with ultrahigh photoresponsivity and fast photoresponse. *Small* **18**, 2200445 (2022).
33. Wu, K. et al. Highly-efficient heterojunction solar cells based on two-dimensional tellurene and transition metal dichalcogenides. *J. Mater. Chem. A* **7**, 7430–7436 (2019).
34. Dong, H. M. et al. Substrate dependent terahertz response of monolayer WS_2. *Appl. Phys. Lett.* **116**, 203108 (2020).
35. Dash, J. K. et al. A method toward fabricating semiconducting 3R-NbS_2 ultrathin films. *J. Phys. Chem. C.* **119**, 19763–19771 (2015).
36. Dai, Z. J. et al. High mobility 3D Dirac semimetal (Cd_3As_2) for ultrafast photoactive terahertz photonics. *Adv. Funct. Mater.* **31**, 2011011 (2021).
37. Xu, S. J. et al. Transient photoconductivity and free carrier dynamics in a monolayer WS_2 probed by time resolved Terahertz spectroscopy. *Nanotechnology* **30**, 265706 (2019).
38. Li, D. et al. Ultrafast dynamics of defect-assisted auger process in $PdSe_2$ films: synergistic interaction between defect trapping and auger effect. *J. Phys. Chem. Lett.* **13**, 2757–2764 (2022).
39. Cocker, T. L. et al. Microscopic origin of the Drude-Smith model. *Phys. Rev. B* **96**, 205439 (2017).
40. Mithun, K. P. et al. Ultrafast dynamics of Dirac surface and bulk photocarriers in topological-insulator bismuth telluride nanocrystals using terahertz spectroscopy. *Phys. Rev. B* **105**, 144302 (2022).
41. Mithun, K. P. et al. Ultrafast time-resolved carrier dynamics in tellurium nanowires using optical pump terahertz probe spectroscopy. *Nanoscale* **15**, 12670–12678 (2023).
42. Li, Q. et al. Active graphene–silicon hybrid diode for terahertz waves. *Nat. Commun.* **6**, 7082 (2015).
43. Glover, R. E. & Tinkham, M. Transmission of superconducting films at millimeter-microwave and far infrared frequencies. *Phys. Rev.* **104**, 844–845 (1956).
44. Suo, P. et al. Observation of negative terahertz photoconductivity in large area type-II Dirac semimetal $PtTe_2$. *Phys. Rev. Lett.* **126**, 227402 (2021).
45. Qin, F. L. et al. Contact engineering high-performance ambipolar multilayer tellurium transistors. *Nanotechnology* **31**, 115204 (2020).
46. Sun, H. et al. Ultrafast polarization-dependent all-optical switching of germanium-based metaphotonic devices. *Photonics Res.* **8**, 263–270 (2020).
47. Yu, Y. F. et al. Engineering substrate interactions for high luminescence efficiency of transition-metal dichalcogenide monolayers. *Adv. Funct. Mater.* **26**, 4733–4739 (2016).
48. Cheng, M. J., Zhu, Z. Z. & Guo, G. Y. Strong bulk photovoltaic effect and second-harmonic generation in two-dimensional selenium and tellurium. *Phys. Rev. B* **103**, 245415 (2021).